JOURNAL OF MATERIALS SCIENCE 19 (1984) 3255–3265

Plastic deformation of ß and γ phase silver–tin alloys

J. R. ABBOTT, D. R. MILLER, D. J. NETHERWAY
The University of Adelaide, Adelaide, S.A. 5001, Australia

The plastic deformation of β and γ phase silver–tin alloys, which are of significance in the formulation of dental amalgam, has been studied using transmission electron microscopy and electron channelling. Deformation twinning in the ordered orthorhombic γ phase on {0 1 1} planes has been confirmed and another twin plane {2 1 1} has been identified. The γ phase was also found to deform by slip on {0 0 1} and {0 1 0} planes; superlattice dislocations with Burgers vectors 1/2[1 0 0] have been identified on the (0 0 1) plane. The disordered h c p β phase deforms essentially by slip on the basal (0 0 0 1) plane by glide of 1/3⟨$\bar{2}$ 1 1 0⟩ dislocations.

1. Introduction

Silver–tin alloys, especially the γ phase composition, are widely used in the preparation of dental amalgam. In this application the alloys are commonly subjected to plastic deformation which may occur during the preparation of the powders themselves or during the processes of amalgamation and condensation of the amalgam into the tooth cavity. It has been shown elsewhere [1] that in the case of the γ phase alloys the reaction with mercury occurs preferentially along deformation twins and grains boundaries. Previous studies by X-ray diffraction and optical metallography of the structure of γ phase [2] have included reference to the presence of deformation twinning on {0 1 1} planes of the ordered orthorhombic structure. Preferential mercury attack was observed on twins of this type but these experiments also indicated the possibility that another twinning system may in fact exist. The present investigation was therefore undertaken to investigate deformation twinning and slip in the γ phase. This involves the interpretation of large numbers of electron micrographs and electron diffraction data, which for orthorhombic crystals is far more complex than for cubic or hexagonal crystals because of the greatly increased number of possible reflections. In order to reduce the complexity of these crystallographic analyses computer aided indexing procedures can be adopted and further simplification can be achieved by the application of the technique of electron channelling. These techniques will be described below.

This study was extended to include the adjacent β phase which has a disordered h c p structure, since these alloys are also of importance in the formulation of dental amalgam.

2. Experimental techniques

The experimental alloys were prepared as bars approximately 10 mm in diameter by vacuum melting high purity silver (99.99%) and tin (99.9%) in evacuated silica capsules at 1000° C and rapidly solidifying by quenching into water. The bars were then subjected to an homogenizing heat treatment for 72 h at a temperature appropriate to the composition of the alloy. The uniformity of the microstructure produced by this homogenization was established by metallographic examination using techniques described previously [1]. Specimens for transmission electron microscopy were prepared from 3 mm diameter discs by electropolishing and ion beam thinning. The γ phase alloys are quite brittle and display mainly intergranular fracture, so that single crystals could readily be extracted from a bar of alloy which had been fractured in compression. These crystals were suitable for mounting directly into the double tilt goniometer stage of a JEOL 120CX electron microscope. This instrument was equipped with a secondary elec-

0022–2461/84 $03.00 + .12

tron detector and a scanning attachment with a "rocking" mode of operation which enabled selected area electron channelling patterns to be obtained from the single crystals.

3. The β and γ phases

Detailed studies of the constitution of silver–tin alloys were first published in 1926 by Murphy [3] and the now widely accepted silver–tin phase diagram (e.g. Hansen [4]) is based essentially on that work. The system displays two peritectic reactions which result in the formation of phases designated β and γ at alloy compositions 14.5 wt% Sn and 26.7 wt% Sn respectively. The corresponding peritectic temperatures are 724° C for the β phase and 480° C for the γ phase. A eutectic reaction is also observed at a temperature of 221° C and an alloy composition 96.5 wt% Sn.

The β phase is a solid solution which spans the composition range 12.8 to 19.5 wt% Sn at room temperature and has a disordered h c p structure. The lattice parameters of a homogeneous β phase alloy containing 18.0 wt% Sn were determined to be $a = 0.2941$ and $c = 0.4778$ nm using powder X-ray diffraction techniques.

The γ phase is a solid solution spanning the composition range 26.0 to 26.7 wt% Sn at room temperature. It should be noted that the upper limit of this phase field was found by the present authors to be 26.7 wt% Sn [1] and not 26.85 wt% Sn, corresponding to the stoichiometric formula Ag_3Sn, as was previously believed. In alloys formulated to have composition 26.85 wt% Sn, the Ag–Sn eutectic reaction product, 96.5 wt% Sn, was found to be present along the grain boundaries of the γ phase. The γ phase belongs to the orthorhombic space group D_{2h}^{13} (No. 59) and at the tin edge of the phase field has lattice parameters $a = 0.5968$, $b = 0.4780$ and $c = 0.5184$ nm [2]. A representation of the (0 1 0) plane in the γ phase, based on the assumption of perfect ordering, is shown in Fig. 1. Because the γ phase exists over a range of composition which does not include the fully ordered structure this assumption is not wholly valid. Nevertheless Fig. 1 displays the principle features of the structure. The orthorhombic unit cell is shown on the left-hand side of Fig. 1. This structure can be related to a slightly distorted h c p unit cell, as shown on the right-hand side of Fig. 1, by the following matrix equation

$$\mathbf{a}_o = \begin{bmatrix} 0 & 2 & 0 \\ 0 & 0 & 1 \\ 2 & 1 & 0 \end{bmatrix} \mathbf{a}_h$$

Note that the orthorhombic b axis corresponds to the hexagonal c axis.

The distortion of the h c p cell introduced by the ordering is approximately 0.3%, and this can be detected as splitting of peaks in X-ray powder diffraction spectra of the γ phase [5, 6], although its magnitude is so small that it would not be expected to be detected in Kikuchi patterns, electron diffraction patterns or in electron channelling patterns. However, because the γ phase is ordered, superlattice reflections of low intensity are present in electron diffraction patterns from suitable orientations. The presence of these superlattice reflections enables the orthorhombic γ phase structure to be readily distinguished from an h c p structure from which no superlattice reflections would occur.

These same considerations also enable the γ phase to be distinguished from the adjacent and closely related h c p β phase. As shown in Fig. 2, a transmission electron diffraction pattern of the [0 1 0] zone in the γ phase, Fig. 2a, contains both the strong fundamental "hexagonal" reflections and the much weaker superlattice reflections which are due to the ordering of the silver and tin atoms. The diffraction pattern from the equivalent zone [0 0 0 1] for the β phase is shown in Fig. 2b. The β phase, having a disordered h c p structure, displays only the strong reflections of Fig. 2a.

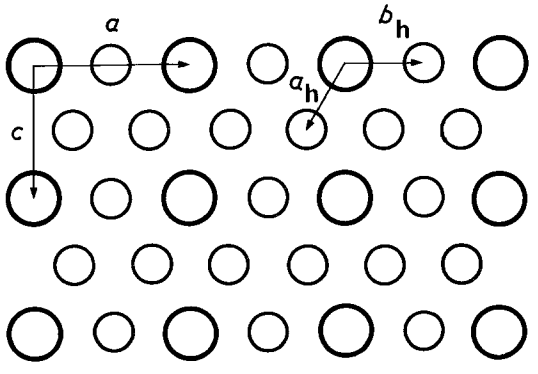

Figure 1 An [0 1 0] projection of the fully ordered γ phase structure. Large and small circles represent tin and silver atoms, respectively.

4. Identification of deformation twins in the γ phase using electron channelling techniques

In the scanning electron microscope electron channelling patterns are formed when the incident

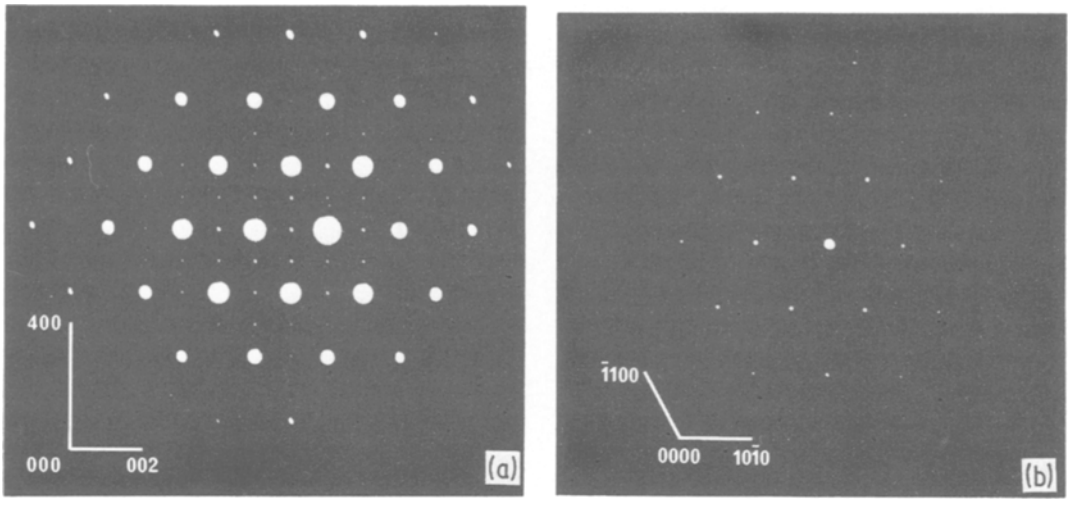

Figure 2 Electron diffraction patterns for (a) the [0 1 0] zone in the γ phase displaying the low intensity superlattice reflections and (b) the [0 0 0 1] zone in the β phase.

beam of electrons is rocked through a solid angle about a point on a crystalline surface so that each point of the image corresponds to a particular angle of incidence [7]. Channelling patterns for the [0 1 0] and [1 0 0] zones of the γ phase are shown in Fig. 3. The origin of the intensity variations in the electron channelling patterns can be considered to result from variations of the effective absorption coefficient for a dynamical diffraction condition. The absorption process frequently involves the production of secondary electrons. When the angle of incidence of the electron beam is near the Bragg angle for a strong reflection the effective absorption coefficient is decreased and the primary beam penetrates further into the crystal. There is then a reduction of the number of secondary electrons produced near enough to the surface to allow them to escape and be detected. Hence the image formed by displaying the signal obtained by collecting secondary electrons shows a pattern similar to the more familiar Kikuchi line patterns obtained using transmission electron microscopy.

The symmetry of these electron channelling

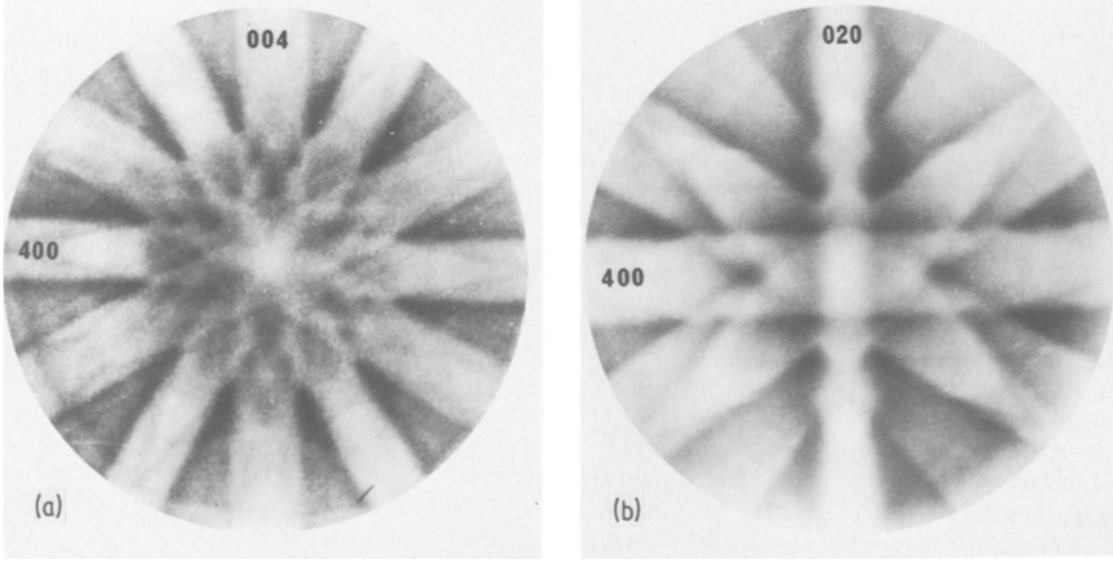

Figure 3 Channelling patterns for (a) the [0 1 0] zone and (b) the [1 0 0] zone in the γ phase.

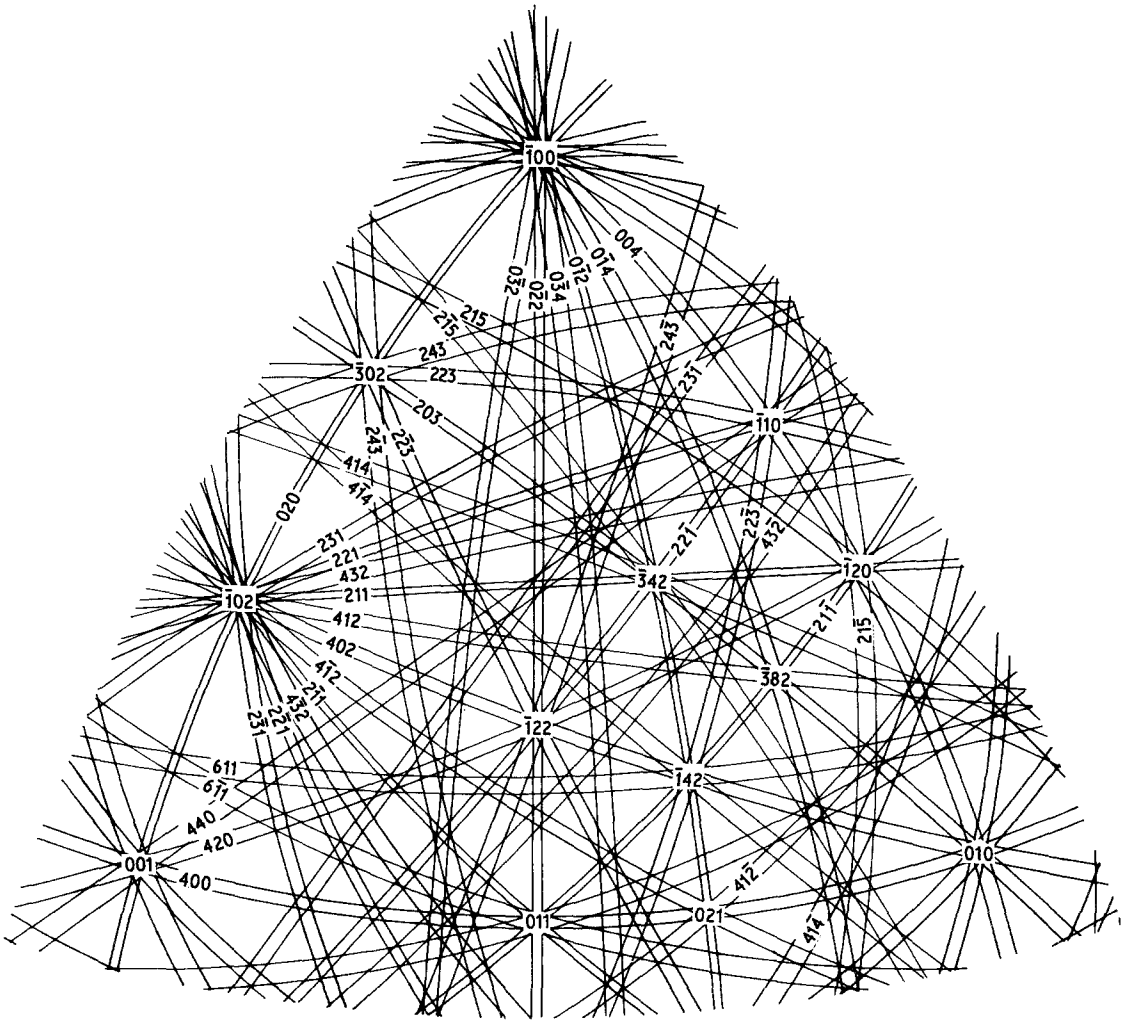

Figure 4 Electron channelling/Kikuchi map for the β and γ phases (indexed according to the unit cell of the orthorhombic γ phase).

patterns (ECPs), like that of the Kikuchi patterns, is determined by the diffracting conditions within the crystal and can be used in a similar way to determine the crystallographic orientation of the crystal. ECP's are particularly useful as they enable the orientation of a bulk specimen to be determined, whereas transmission electron microscopy (TEM) is limited to specimens whose thickness is of the order 100 nm. The orientation of specimens is readily determined by referring the ECP to a channelling map, since the angular range covered by the pattern is of the order of 20°, which is significantly greater than the 7° typical of a Kikuchi pattern.

Channelling maps can, like Kikuchi maps, be produced by assembling a montage of separate patterns over the range of orientations of interest. It is often more convenient, however, to calculate the nature of the channelling patterns using a computer. In Fig. 4, the [$\bar{1}$ 1 1] ECP map for the γ phase of the Ag–Sn alloy systems is shown. Here structure factors were derived from the electron scattering factors for Ag and Sn of Doyle and Turner [8]. In order to simplify the map and to permit it to be more directly related to experimentally observed ECPs only those reflections whose structure factor was greater than 1/3 of the strongest reflection (0 2 0) have been included and further, since in practice the (0 0 2) and (2 0 1) lines are too diffuse to be recognised these have been omitted and the sharper (0 0 4) and (4 0 2) lines have been included instead.

A [$\bar{1}$ 1 1] stereographic projection was chosen, as opposed to say an [0 1 0], since less distortion

TABLE I Comparison of the d spacings and structure factors of related reflections in the β and γ phases

hkl*	d($\times 10^{-1}$ nm)	$\lvert F_{hkl}\rvert^2$
0 0 2	2.592	493
2 0 1	2.586	487
1 0 $\bar{1}$ 0	2.547	503
0 2 0	2.390	1759
0 0 0 2	2.389	1848
0 1 2	2.279	1228
2 1 1	2.275	1231
1 0 $\bar{1}$ 1	2.248	1273
0 2 2	1.757	273
2 2 1	1.755	270
1 0 $\bar{1}$ 2	1.743	284
2 0 3	1.495	797
4 0 0	1.492	798
1 1 $\bar{2}$ 0	1.471	821
0 3 2	1.357	487
2 3 1	1.357	489
1 0 $\bar{1}$ 3	1.350	513

*The four-figure entries in the first column are the Miller-Bravais indices $hkil$ used for the β phase. The three-figure entries are the Miller indices used for the γ phase.

of the quadrant occurs. This map can also be used as a Kikuchi map, and indeed for the map shown in Fig. 4 widths of the bands were computed on the basis of an assumed accelerating potential of 120 kV used in the transmission mode instead of the 40 kV used in the scanning mode. This means that the bands are somewhat narrower so that the reduced overlap makes recognition easier.

It should be observed that a rotation of 60° about [0 1 0] brings the channelling map into coincidence with itself. For example, [$\bar{1}$ 0 0] and [$\bar{1}$ 0 2], [0 0 1] and [$\bar{3}$ 0 2], and [0 1 1] and [$\bar{3}$ 4 2] are pairs of patterns which appear identical. (This is also true for Kikuchi patterns. However, the presence of the weak superlattice reflections in the diffraction patterns of the ordered γ phase alloys allows differentiation.) The structure factors and d spacings for hexagonally related reflections are very close, see Table I, so that the 0.3% deformation of the hexagonal cell is not discernible in the channelling patterns, and since the superlattice reflections are too weak to produce observable channelling contrast, there is alway s a 60° ambiguity in indexing. The structure factors (multiplied by the appropriate volume factor) and d spacings of equivalent reflections in the β phase (18.0 wt% Sn) are also given in Table I. The similarity implies that the channelling map may also be used for the β phase alloy after suitably transforming the indices.

As the quality of ECPs is particularly sensitive to the perfection of the crystal and surface quality [7] the low ductility and intergranular mode of failure of the γ phase alloy make it a particularly suitable material from which to obtain ECPs.

Crystals of γ phase were tilted in the electron microscope so that the trace of the deformation markings of interest did not deviate on passing from one surface to the other, as in Fig. 5. This means that the pole of the habit plane of the

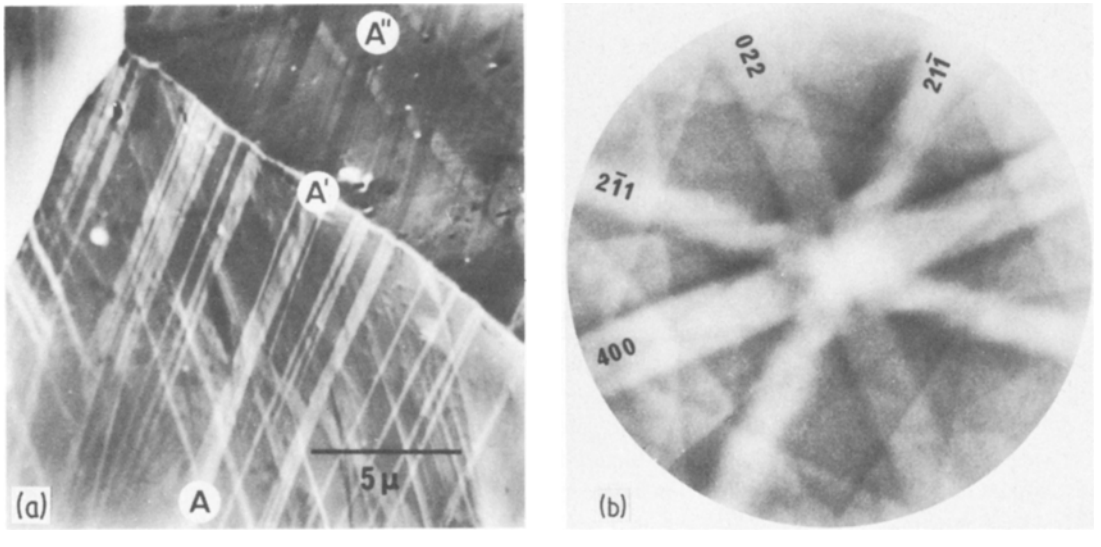

Figure 5 (a) Single crystal with one set of deformation markings appearing straight across two surfaces, and (b) its corresponding electron channelling pattern. The traces AA'A" clearly lie on (2 1 $\bar{1}$) planes.

deformation markings was normal to the electron beam direction. In other words, the habit plane belongs to the zone in the centre of the corresponding ECP. After alignment of the ECP with the image using a rotation calibration, the habit plane could be then identified directly from the ECP without requiring a detailed two-surface analysis to be carried out. For example, from Figs. 5a and b it can be immediately seen that the habit plane of the traces $AA'A''$ is $(2\,1\,\bar{1})$.

Using these electron channelling techniques, twinning has been identified on $\{0\,1\,1\}$ and $\{2\,1\,1\}$ planes of the orthorhombic γ phase. As previously noted, due to the indexing ambiguity these planes could have been identified as $\{2\,2\,1\}$ and $\{0\,1\,2\}$, respectively. However, in the transmission electron microscope, where the superlattice reflections allow differentiation, only $\{0\,1\,1\}$ and $\{2\,1\,1\}$ twins have been observed. The channelling patterns were indexed to conform to the twin types identified by TEM.

5. Transmission electron microscopy of the β and γ phases

5.1. Indexing electron diffraction patterns

Owing to the large unit cell size and orthorhombic space group of the γ phase there are many possible reflections that could be attributed to a particular measured d spacing within the limits of accuracy of experimental measurement. It frequently arises, therefore, that many possible solutions to the analysis of a diffraction spot or Kikuchi pattern can be found.

In order to arrive at the correct solution, an experimental technique involving recording electron diffraction patterns from a specimen which is progressively tilted through a series of known angles using the goniometer stage has been found useful. One of these diffraction patterns should contain superlattice reflections for the reasons discussed later. A consistent analysis of this series of three or four diffraction patterns must then be carried out. To undertake this task manually is very tedious, so two computer programs were devised which substantially reduce the time required for this crystallographic analysis.

The first, program ORTHEX, relates to the indexing of spot patterns. The input data required are camera length, distances and angles between diffraction maxima and estimates of relevant experimental errors. The output from the program is presented as a table of possible solutions to the diffraction pattern within the range of experimental error. This program makes allowances for the possibility of double diffraction occurring.

The second, program KORTHU, is used in the more general case of the solution of Kikuchi patterns. In addition to the usual instrumental parameters, the input data required here are distances between pairs of Kikuchi lines, distances between points of intersection of midpoints of Kikuchi pairs and the angles of intersection of these lines. The output from this program includes a list of possible crystallographic indices of the beam direction as well as the corresponding possible indices of the Kikuchi lines.

For the reasons already explained above, this list was very extensive. However, two factors enabled the number of possible solutions to be greatly reduced. Firstly, since only reflections with an intensity greater than about 1% of that of the $(0\,2\,0)$ gave rise to Kikuchi lines which were visible under normal operating conditions, solutions involving those weak reflections were able to be deleted from the output of the program. Secondly, possible solutions involving ambiguities arising from the identical nature of Kikuchi patterns from each of the 30° sectors within the 90° quadrant, as shown in Fig. 4, could be resolved by carrying out suitable tilting experiments in the electron microscope. These involved the determination of the proximity of a particular Kikuchi pattern to a spot diffraction pattern containing superlattice reflections. An example of this indexing procedure is given in the next section.

5.2. Twinning in the γ phase

Deformation twins in the γ phase have been reported to occur on $\{0\,1\,1\}$ planes [2] and also on $\{1\,1\,1\}$ planes [6]. In both cases the crystallography was carried out using X-ray diffraction techniques. In this laboratory, using transmission electron microscopy, deformation twinning on $\{0\,1\,1\}$ planes has been confirmed and another deformation twinning system lying on $\{2\,1\,1\}$ planes has been observed. In both cases it was established that the orthorhombic ordering is maintained within the twins by obtaining diffraction patterns with superlattice reflections from within the twins themselves.

A bright field image of a twin is shown in Fig. 6. The solution to the crystallogaphic problem of identifying the nature of the twin involves indexing diffractions patterns from both the twin

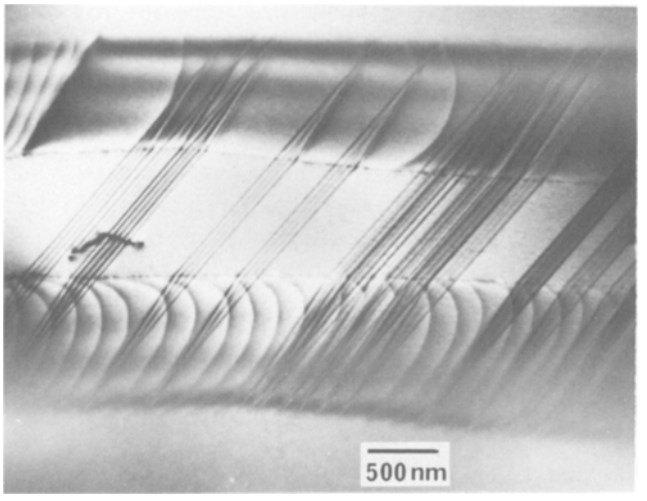

Figure 6 Bright field image of a $(\bar{2}\,1\,1)$ twin with $(0\,1\,0)$ stacking faults within the twin and dislocations in the twin boundaries.

and matrix using the procedure outlined above. The Kikuchi pattern in Fig. 7, obtained from within the twin, was analysed using program KORTHU and, in this case, only three viable solutions were found. These solutions are indicated on Fig. 7. Each Kikuchi pattern may be indexed into four equivalent quadrants, the four remaining quadrants being mirror images. Initially solutions (a) and (c) were indexed into the $\bar{h}\,k\,l$ quadrant while solution (b) was indexed into the $h\,k\,l$ quadrant. If the γ phase was hexagonal then these three solutions would be identical and could have been indexed into the usual 30° sector for hexagonal symmetry. However, to resolve the ambiguity it was found that the [1 0 0] diffraction pattern was recorded to be 24° away from the Kikuchi pattern being analysed. This [1 0 0] diffraction pattern was able to be distinguished from the [1 0 2] pattern by the presence of the superlattice reflections marked with arrows in Fig. 8.

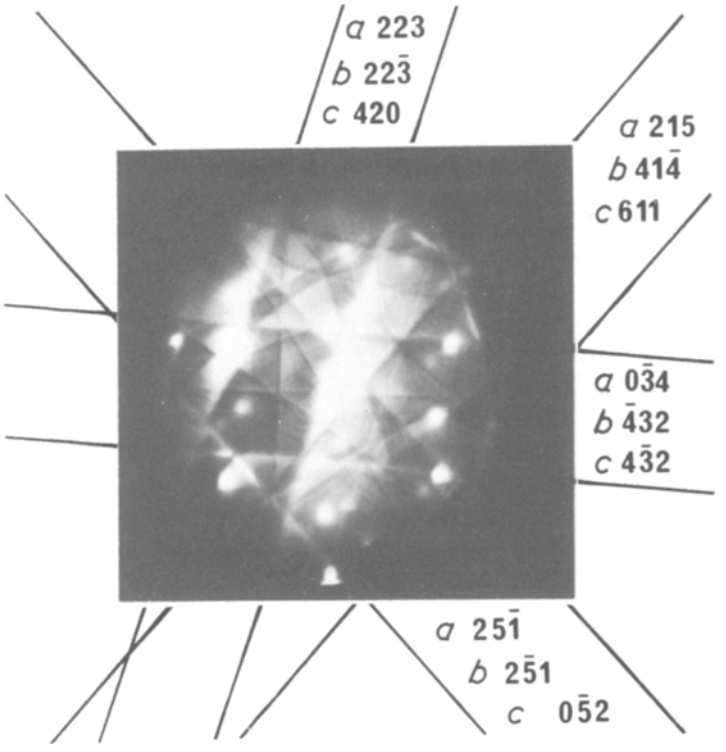

Figure 7 A Kikuchi pattern from the twin showing the three independent solutions found.

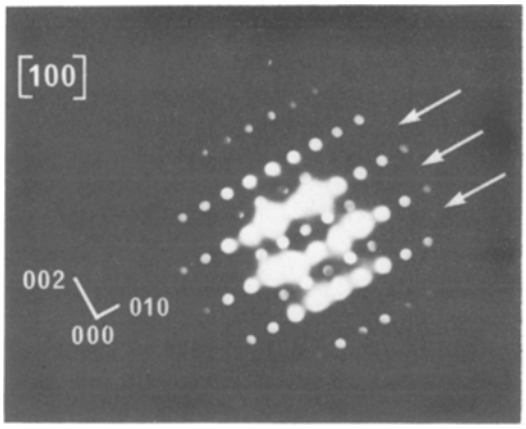

Figure 8 Diffraction pattern for the [1 0 0] zone from the twin used to determine the crystal orientations relative to the superlattice. The arrows indicate rows of superlattice reflections which would be absent in the [1 0 2] zone.

The calculated angles to [1 0 0] for solutions (a), (b) and (c) were 25°, 47° and 77°, respectively, so that solution (a) was unequivocally determined as being the correct solution. The other diffraction patterns from the twin could be readily indexed in a similar fashion.

The series of diffraction patterns obtained from the matrix were indexed using the [0 1 1] diffraction pattern, which contains superlattice reflections, as the reference zone. By choosing to index these diffraction patterns from the matrix into the $\bar{h}\,k\,l$ quadrant there is no loss of generality since the other three quadrants into which they could have been indexed are identical. In determining the crystallographic relationship of the twin to the matrix, however, it is necessary to consider the four equivalent sets of solutions to the series of twin diffraction patterns. The positions of these are shown on Fig. 9 on a $(\bar{2}\,1\,1)$ stereographic projection. By examining the relationships between the patterns from the twin and the matrix the series marked with a star is clearly correct. The twin is a 180° rotation of the matrix about the $(\bar{2}\,1\,1)$ pole.

The pole of the habit plane was determined by tilting the specimen in the microscope about the trace of the twin boundary and by using the projected widths of this boundary, the angle to its pole was calculated. The pole of the habit plane was found in this manner to be also $(\bar{2}\,1\,1)$.

Although the habit plane and crystallographic relationship of the twin to the matrix have been determined the magnitude and direction of the

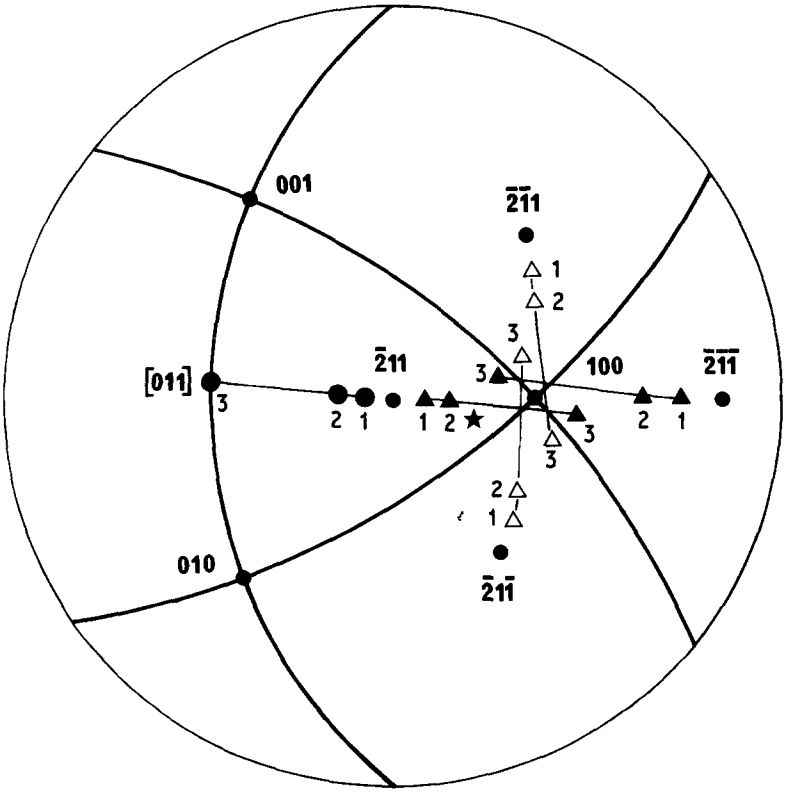

Figure 9 A $(\bar{2}\,1\,1)$ stereographic projection indicating the orientation of three successive diffraction patterns obtained from both the twin and matrix. Numbered circles indicate the orientations of the matrix whereas the triangles indicate the four crystallographically equivalent sets of solutions for the orientations of the twin. The open triangles indicate that the point is located 180° away, on the other side of the projection.

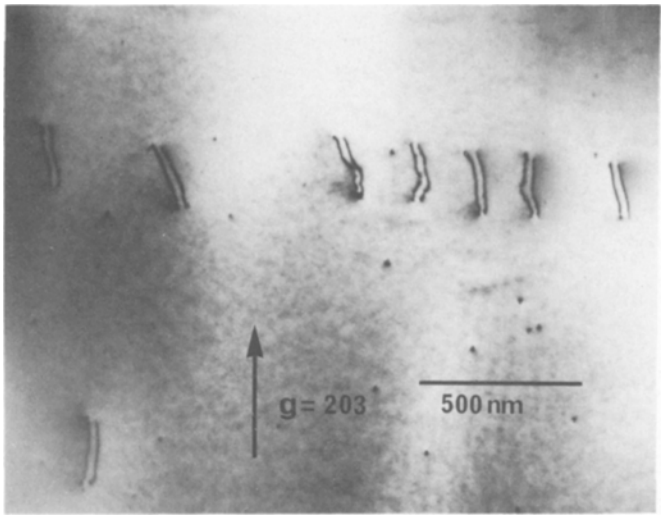

Figure 10 An (0 0 1) slip band in the γ phase with superlattice dislocations having Burgers vector 1/2[1 0 0].

twinning shear cannot be resolved in the transmission electron microscope. However, it is expected that the (2 1 1) twins found in the γ phase would have twin elements $K_1 = (2\,1\,1)$, $\eta_1 = [\bar{3}\,8\,\bar{2}]$, $K_2 = (\bar{2}\,3\,\bar{1})$, $\eta_2 = [9\,8\,6]$ with a twinning shear of $S = 0.114$. These elements were derived from the related twin elements $K_1 = (0\,1\,\bar{1}\,1)$, $\eta_1 = [0\,\bar{1}\,1\,2]$, $K_2 = (0\,\bar{1}\,1\,3)$, $\eta_2 = [0\,3\,\bar{3}\,2]$, $S = [(c/a)^2 - 9/4]/[(c/a)\sqrt{3}]$ from the h c p structure [9]. The twin elements for {0 1 1} twins were found to be $K_1 = (0\,\bar{1}\,1)$, $\eta_1 = [0\,\bar{1}\,\bar{1}]$, $K_2 = (0\,1\,1)$, $\eta_2 = [0\,\bar{1}\,1]$, $S = 0.168$ [2], and these are similarly related to the twin elements in the h c p structure $K_1 = (1\,0\,\bar{1}\,\bar{2})$, $\eta_1 = [\bar{1}\,0\,1\,\bar{1}]$, $K_2 = (1\,0\,\bar{1}\,\bar{2})$, $\eta_2 = [1\,0\,\bar{1}\,1]$, $S = 0.169$ for zirconium, for example.

Twins on both {0 1 1} and {2 1 1} planes were accompanied by stacking faults lying on (0 1 0) planes within the twins, as in Fig. 6. These are similar to the stacking faults in the basal plane of h c p metals which have been observed within twins in magnesium, beryllium and titanium [10]. As can be seen in Fig. 6 there is a high dislocation density within the twin boundaries which may account for the high reactivity of these regions towards mercury [1].

It should be noted in passing that deformation twinning in the γ phase of the Ag–Sn system appears to be restricted to the {0 1 1} and {2 1 1} planes. The fact that it has not been observed on the crystallographically related {2 2 1} and {0 1 2} planes, respectively, would appear to be a consequence of the ordering in the alloy.

While twinning on {0 1 1} planes has been confirmed and twinning on {2 1 1} planes has been discovered using both transmission electron microscopy and electron channelling techniques, no twins on {1 1 1} planes have been identified. This is perhaps not surprising as {1 1 1} planes in the orthorhombic system are related to the $\{1\,2\,\bar{3}\,4\}$ planes in an h c p structure and these would appear to be unlikely planes on which twinning would occur.

5.3. Slip in the γ phase

Slip occurs much less frequently than twinning in the γ phase; however, slip has been observed to occur on (010) planes [1, 11], and on (001) planes, Fig. 10. Slip on (0 1 0) and (0 0 1) planes in the γ phase corresponds to basal slip on (0 0 0 1) and prismatic slip on $(0\,\bar{1}\,0)$ planes, respectively, in hexagonal metals.

Identification of the glide planes was accomplished using the standard technique of rotating the specimen until the slip bands were aligned along the tilt axis of the tilt/rotation goniometer. Then, by tilting, a series of images, along with corresponding diffraction patterns, was obtained. The diffraction patterns were indexed following the previously discussed procedure and calculations based on the projected widths of the dislocations then enabled the angle from the beam direction to the glide plane to be determined. The glide plane could be then identified with the help of a suitable stereographic projection.

Complete invisibility of the dislocations in Fig. 10 occurred for $\mathbf{g} = (0\,2\,0)$ and (0 0 4), Figs. 11a and b, indicating that the Burgers vector

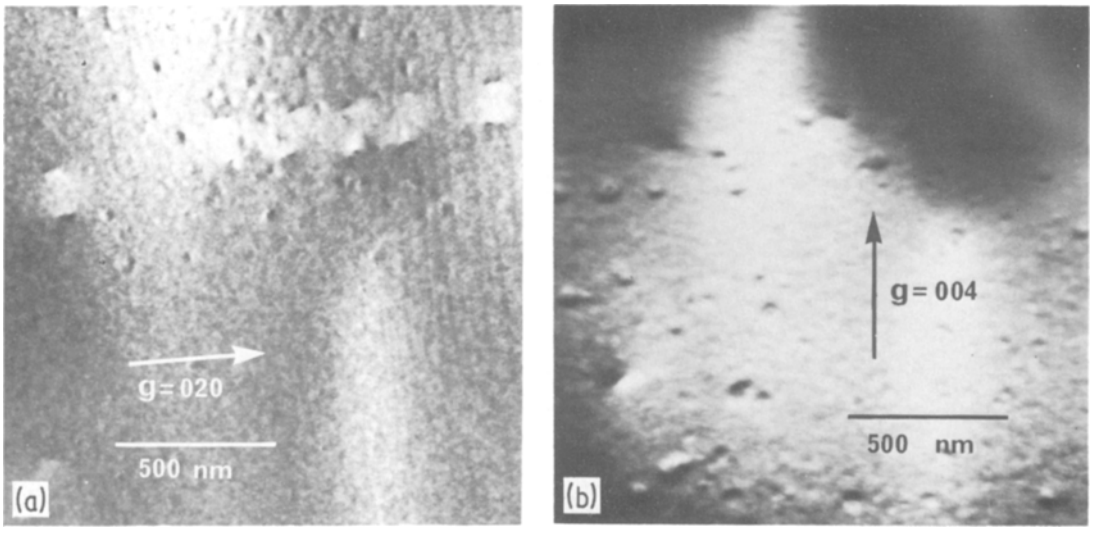

Figure 11 Complete invisibility of dislocations for (a) $\mathbf{g} = (0\,2\,0)$ and (b) $\mathbf{g} = (0\,0\,4)$.

b of the dislocations is $1/2\ [1\,0\,0]$ using the $\mathbf{g}\cdot\mathbf{b} = 0$ invisibility criterion. The dislocations lie roughly in the $[1\,0\,0]$ direction so that they are essentially screw dislocations. Complete invisibility was attained because, being screw dislocations, the conditions $\mathbf{g}\cdot\mathbf{b}_e = 0$ and $\mathbf{g}\cdot\mathbf{bxu} = 0$ were also satisfied, where $\mathbf{b}_e$ is the edge component of the Burgers vector and **u** is the dislocation line direction. The Burgers vector $1/2[1\,0\,0]$ is consistent with $1/3\langle 1\,\bar{2}\,1\,0\rangle$, the Burgers vector for prismatic slip in hexagonal metals.

The dislocations occur in pairs and could be described as superlattice dislocations because $1/2[1\,0\,0]$ is a lattice vector of the "hexagonal" sublattice. This means that there is no stacking fault in the sublattice between the dislocations but rather an antiphase boundary where there is a shift in the ordering of the tin atoms.

5.4. Slip in the β phase

The predominant mode of deformation in the very ductile β phase is slip on basal $(0\,0\,0\,1)$ planes. A typical slip band is shown in Fig. 12 in which the Burgers vector is $1/3[\bar{2}\,1\,1\,0]$ and the dislocation line direction close to $[1\,\bar{2}\,1\,0]$.

In Fig. 13 pairs of dislocations are visible in another $(0\,0\,0\,1)$ slip band. The Burgers vector of the dislocations is also $1/3[\bar{2}\,1\,1\,0]$ while the dislocation line direction is approximately 15° from $[1\,\bar{2}\,1\,0]$. The pairing of dislocations in this

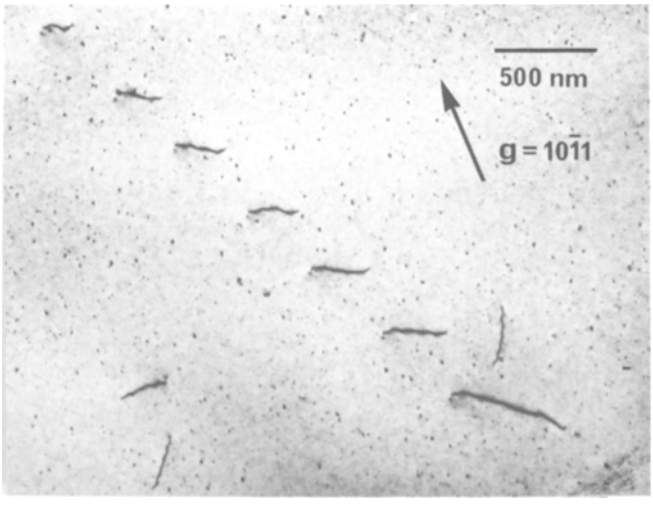

Figure 12 A typical slip band in the β phase lying on the basal $(0\,0\,0\,1)$ plane.

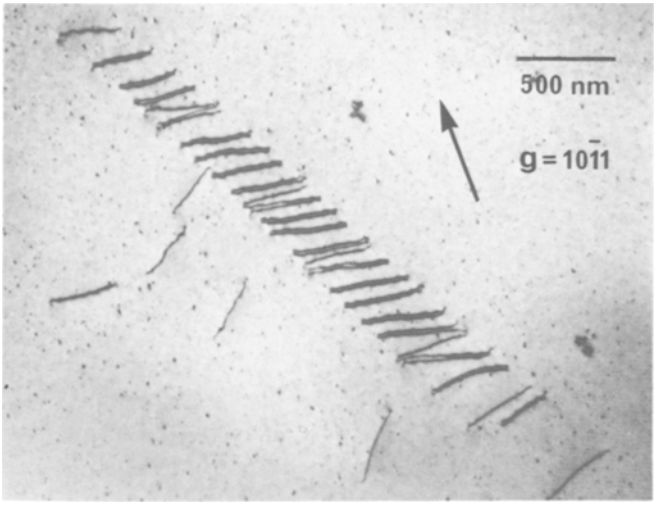

Figure 13 Paired dislocations in the β phase indicative of incipient ordering.

fashion in a slip band is indicative of ordering in the alloy, as in the γ phase dislocations of Fig. 10. Although the β phase is a disordered alloy this suggests that incipient ordering may occur. The slip band immediately to the lower left of the paired dislocations in Fig. 13 lies on a parallel (0 0 0 1) plane. The dislocations have the same Burgers vector, $1/3[\bar{2}\,1\,1\,0]$; however their line direction is close to $[\bar{2}\,1\,1\,0]$.

6. Summary

1. In addition to the previously reported deformation twins on $\{0\,1\,1\}$ planes in γ phase silver–tin alloys, deformation twins have now been identified on $\{2\,1\,1\}$ planes.

2. Superlattice dislocations with Burgers vectors $1/2[1\,0\,0]$ have been identified in the ordered orthorhombic γ phase on (0 0 1) planes.

3. Slip in the disordered β phase has been seen to occur on the basal (0 0 0 1) planes. The Burgers vectors of these dislocations is $1/3\langle\bar{2}\,1\,1\,0\rangle$.

4. Electron channelling techniques proved to be invaluable in crystallographic analyses of bulk specimens.

5. Computer aided indexing of electron diffraction patterns was very effectively applied to reduce the complexity of the crystallographic analyses.

Acknowledgements

This work was carried out with the support of the National Health and Medical Research Council Commonwealth of Australia Grant No. 840299 to Professor D. R. Miller.

References

1. J. R. ABBOTT, D. R. MILLER and D. J. NETHERWAY, *J. Biomed. Mater. Res.* **16** (1982) 535.
2. C. W. FAIRHURST and J. B. COHEN, *Acta Crystallogr.* **B28** (1972) 371.
3. A. J. MURPHY, *J. Inst. Met.* **35** (1926) 107.
4. M. HANSEN, "Constitution of Binary Alloys" (McGraw-Hill, New York, 1958).
5. O. NIAL, A. ALMIN and A. WESTSGREN, *Z. Phys. Chem.* **14** (1931) 81.
6. H. WIRJOSUMATO, R. S. MATEER and C. D. REITZ, *J. Dent. Res.* **52** (1973), special issue, 200.
7. D. E. NEWBURY and H. YAKOWITZ, in "Practical Scanning Electron Microscopy" edited by J. I. Goldstein and H. Yakowitz (Plenum Press, New York, 1975) p. 149.
8. P. A. DOYLE and P. S. TURNER, *Acta Crystallogr.* **A24** (1968) 390.
9. H. S. ROSENBAUM, in "Deformation Twinning" Metallurgical Society Conferences Vol. 25, edited by R. E. Reed-Hill, J. P. Hirth and H. C. Rogers (Gordon and Breach Science Publishers, New York, 1964).
10. P. G. PARTRIDGE, *Met. Rev.* **12** (1967) 169.
11. J. R. ABBOTT, PhD thesis, University of Adelaide (1981).

Received 7 November
and accepted 19 December 1983